Supplemental Materials

Change of Line Tension in Phase-Separated Vesicles upon Protein Binding

Jaime B. Hutchison[†], Robert M. Weis[‡], Anthony D. Dinsmore[†*]

[†]Department of Physics and [‡]Department of Chemistry, University of Massachusetts Amherst

*Correspondence: dinsmore@physics.umass.edu

The binding of poly-L-histidine generates changes in vesicle shape. We examined the generality of the reduction in σ/P due to binding interactions between nickel lipids and histidine by performing similar experiments with poly-L-histidine (5,000 - 25,000 MW) and no GFP. GUVs used in these

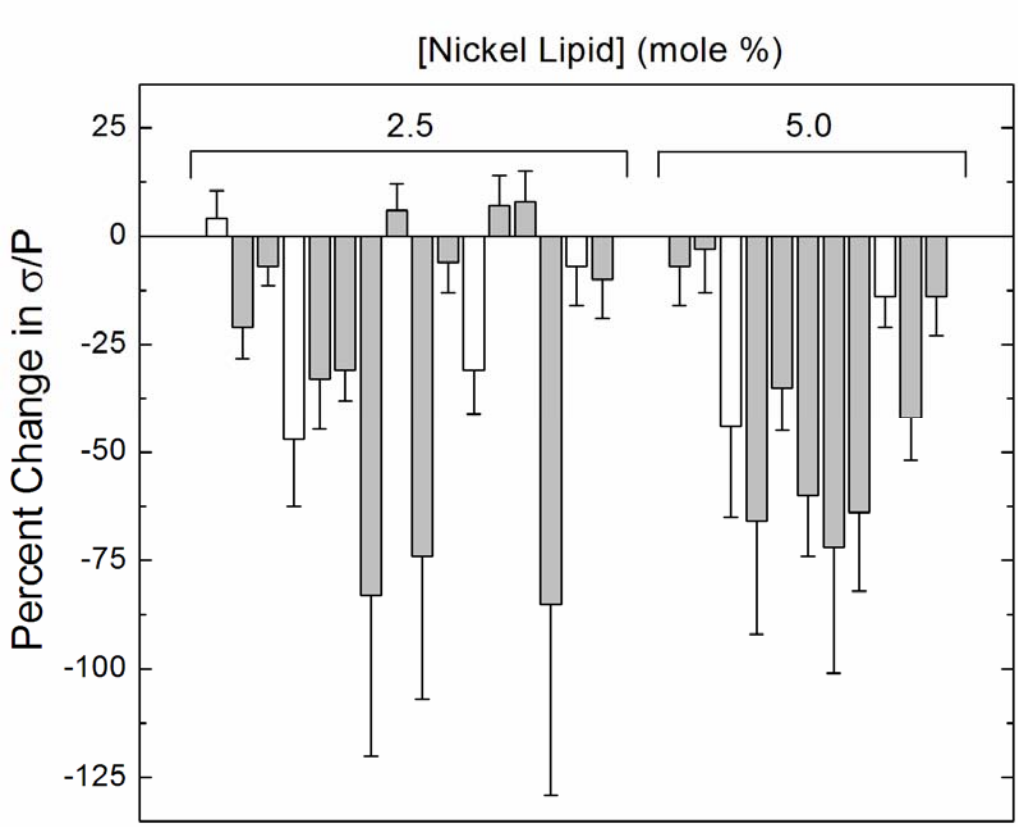

Figure S1. The percent change in line tension over the Laplace pressure (σ/P) from the binding of poly-L-histidine to vesicles containing either 2.5 or 5 mol% nickel lipid. The gray-filled columns are changes in σ/P of vesicles in which the volume remained unchanged, within experimental uncertainty, and the unfilled columns are vesicles that underwent a discernible change in volume upon binding poly-L-histidine.

experiments were composed of 2:2:1 DOPC:PSM:Chol with either 2.5 or 5 mol% nickel lipid. As shown in Figure S1, of the 16 experiments performed with 2.5 mol% nickel lipid, 12 resulted in no change in volume and corresponded to an average decrease of σ/P of 27 ± 10%. Of the 11 experiments performed with 5 mol% nickel lipid, nine resulted in no change in volume and corresponded to an average decrease of σ/P of 40 ± 9%. This observation is consistent with the idea that it is the chelation of nickel lipid by the hexahistidine tag (independent of GFP) that generates the decrease in σ/P, and that the larger valency of poly-L-histidine produces a greater change in σ/P.

No observed effect of GFP binding on vesicle surface area. We investigated the possibility that binding of his-tagged GFP could generate a change in membrane area, which could contribute to shape changes in the two-phase system. We performed control experiments with single-phase vesicles (L_o) and monitored total vesicle area before and after GFP binding. For these experiments, vesicles composed of DOPC with 10 mol% nickel lipid were used. The results in Figure S2 show that the total area did not change, within the uncertainty of our measurements.

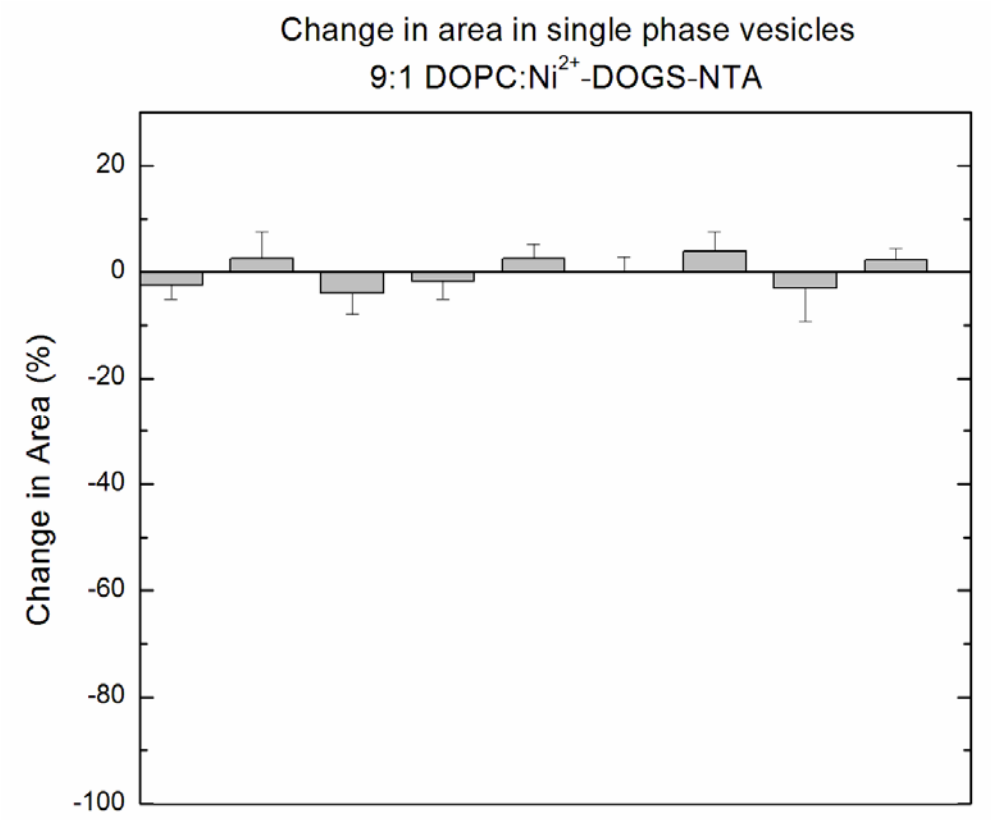

Figure S2. Measured percent change in area of single-phase vesicles containing 10% nickel lipid resulting from GFP binding.

Image deconvolution provides evidence of accumulation of bound GFP at the L_o/L_d boundary. We hypothesize that the observed reduction in line tension upon the binding of his-tagged GFP to phase-separated GUVs is due to protein-lipid clusters accumulating preferentially at the boundary between the L_o and L_d phases. Here we describe experiments that use fluorescence imaging to probe for enhanced GFP concentration at the boundary. Giant unilamellar vesicles (GUVs) with 2:2:1 DOPC:PSM:Chol and 1 mol% nickel lipid were incubated with his-tagged GFP, centrifuged at 4,500 x *g*, and then resuspended in sucrose. This last step removed unbound GFP, thereby reducing the background fluorescence and improving image contrast. However, as a result of this procedure, we could not correlate the buildup of fluorescence intensity with a reduction of line tension. In this analysis, we have included vesicles that have more than one L_d domain (*i.e.*, multiple L_o/L_d boundaries).

GUVs were imaged using a 63x oil-immersion objective in epifluorescence mode with a CoolSNAP HQ^2 CCD camera (Photometrics Inc., Tucson, AZ). Images were deconvolved with Huygens Essential software (Scientific Volume Imaging BV, Hilversum, NL) and surface plots of intensity were created with ImageJ.[S1]

Figures S3-S8 show the original and deconvolved fluorescence images of six vesicles containing 1 mol% nickel lipid. GFP is bound to the nickel lipid partitioned into the L_d phase, so the L_o phase appears dark. The vesicles thus have the appearance of a bite taken out at the location(s) of the L_o domain(s). In the Figures S3 to S8, panel A is the original image, panel B is the deconvolved image, and panel C is a surface plot of the intensity in the deconvolved image. Each image shows some evidence of enhanced fluorescence at the L_o/L_d boundary. The shapes of the vesicles are varied and some appear to have vesicles captured inside them, which we think may have occurred during the process of sedimentation and resuspension. Despite the fact that the enhancement is not the same in all vesicles, and that there is more noise in some images than others, all the images show enhanced GFP emission from the L_o/L_d boundary.

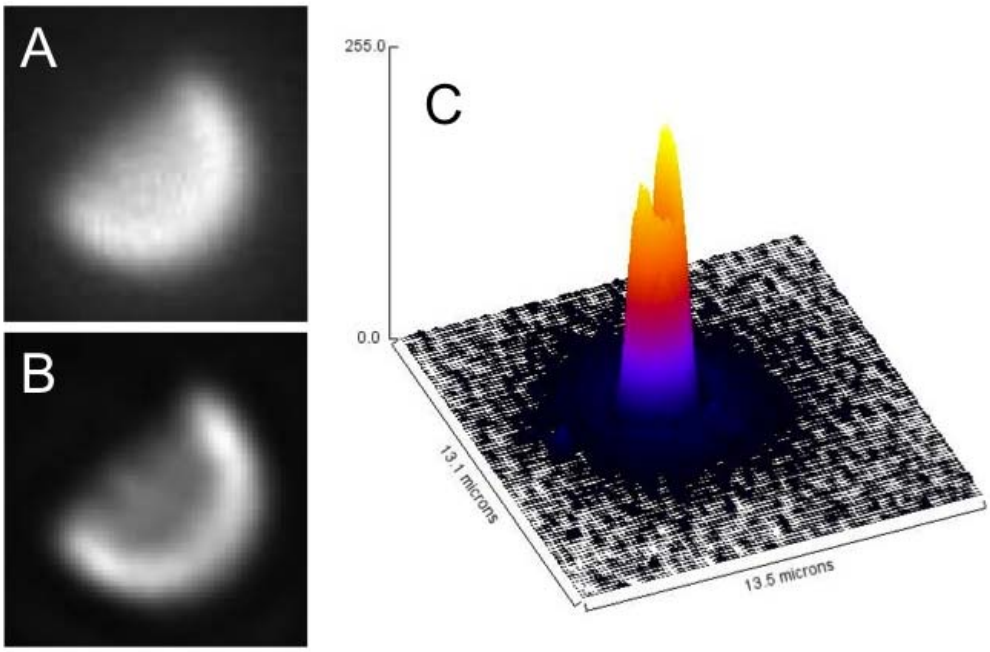

Figure S3. Deconvolution analysis of GFP fluorescence (1 mol% nickel lipid). (A) Original image. (B) Deconvolved image. (C) Surface plot of intensity in deconvolved image; scale is arbitrary.

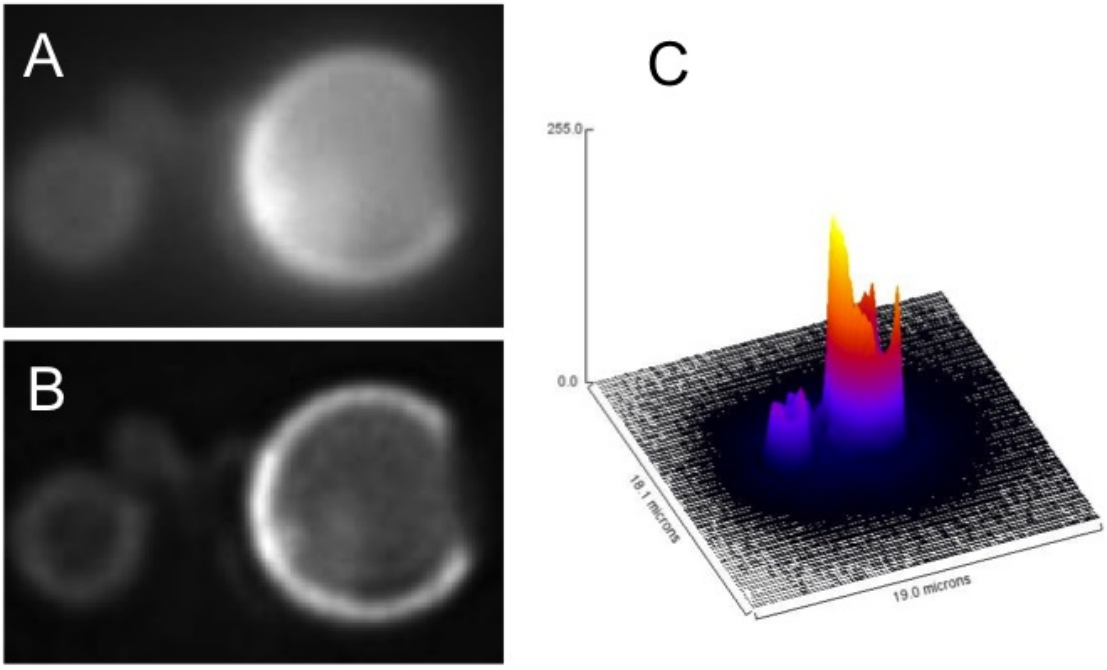

Figure S4. Deconvolution analysis of GFP fluorescence (1 mol% nickel lipid). (A) Original image. (B) Deconvolved image. (C) Surface plot of intensity in deconvolved image; scale is arbitrary.

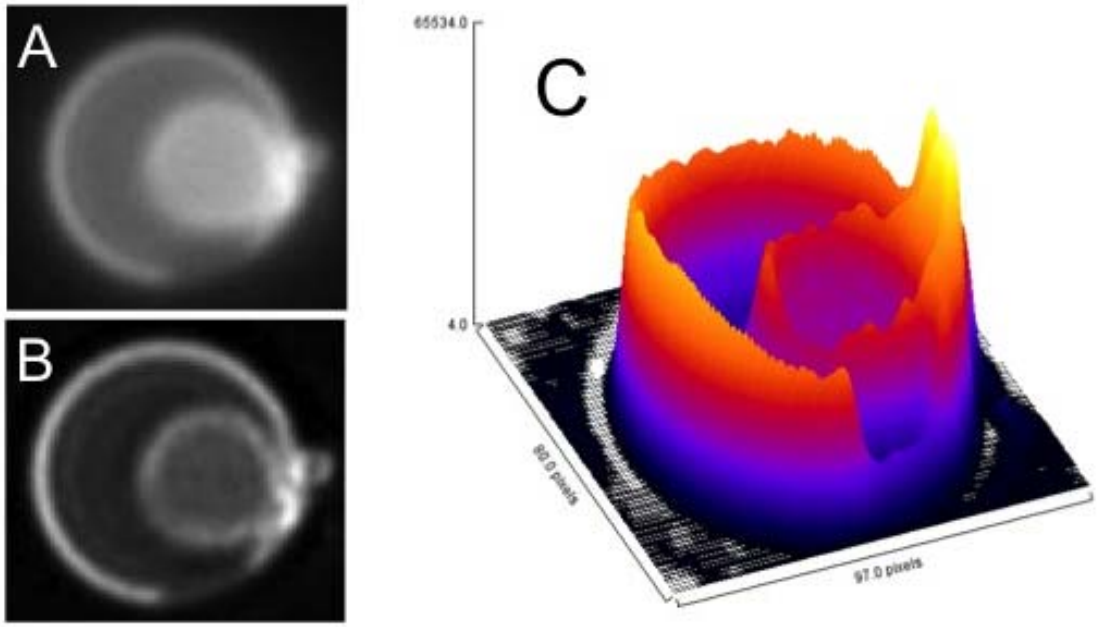

Figure S5. Deconvolution analysis of GFP fluorescence (1 mol% nickel lipid). (A) Original image. (B) Deconvolved image. (C) Surface plot of intensity in deconvolved image; scale is arbitrary.

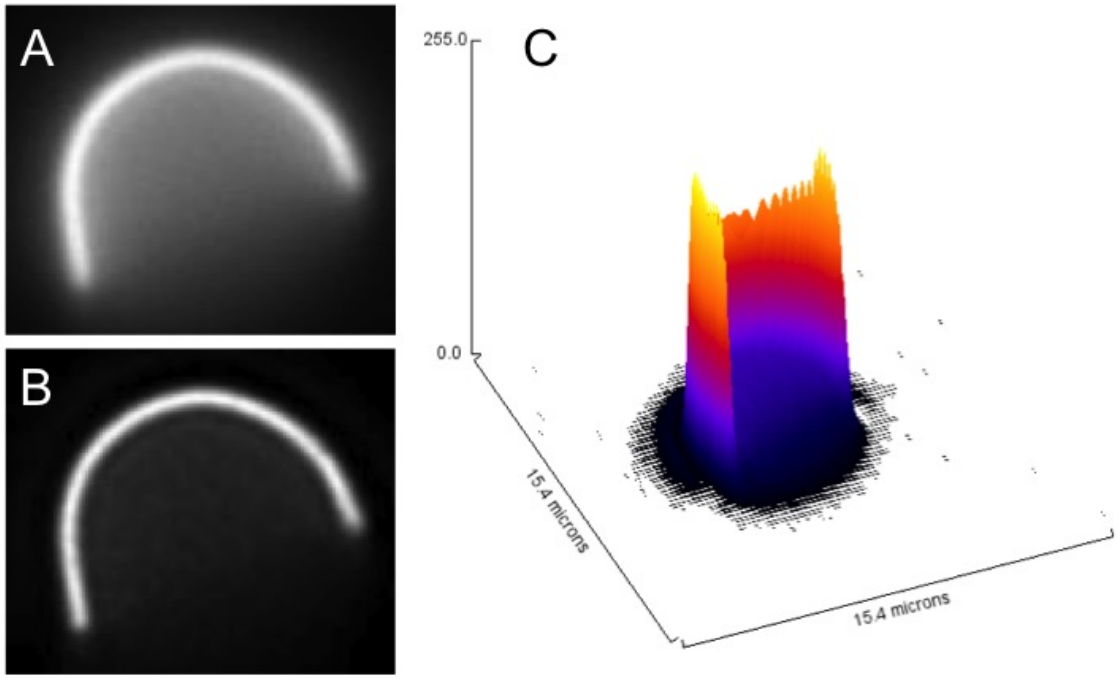

Figure S6. Deconvolution analysis of GFP fluorescence (1 mol% nickel lipid). (A) Original image. (B) Deconvolved image. (C) Surface plot of intensity in deconvolved image; scale is arbitrary.

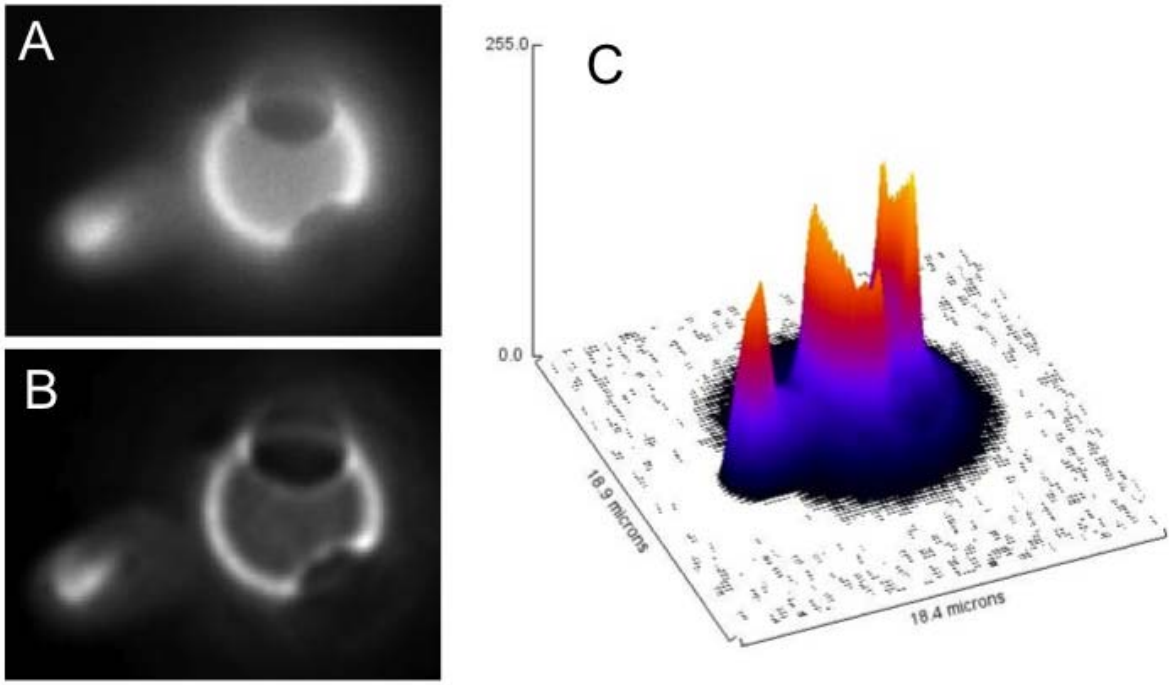

Figure S7. Deconvolution analysis of GFP fluorescence (1 mol% nickel lipid). (A) Original image. (B) Deconvolved image. (C) Surface plot of intensity in deconvolved image; scale is arbitrary.

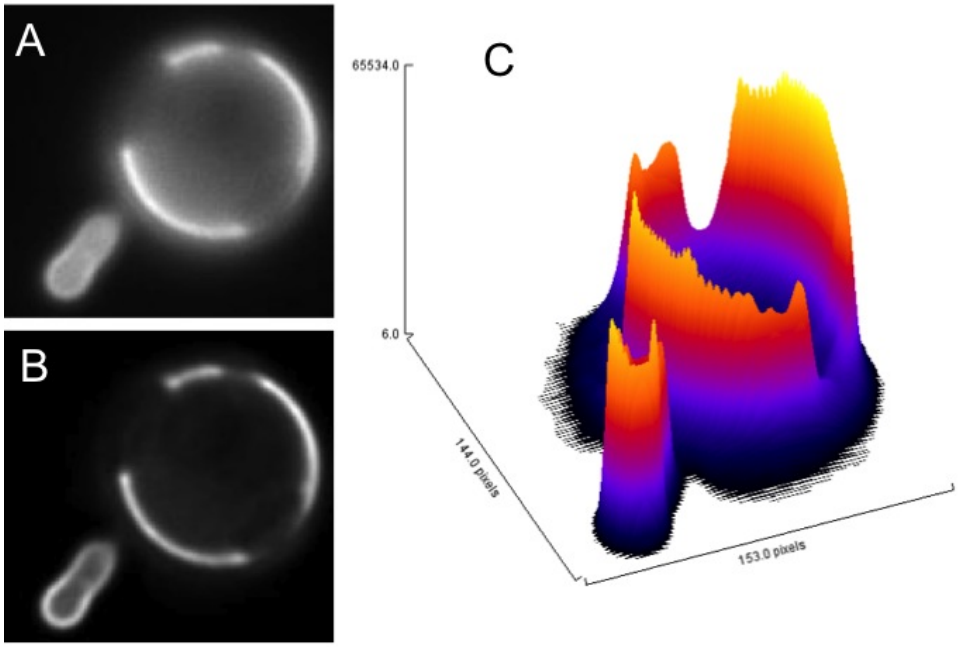

Figure S8. Deconvolution analysis of GFP fluorescence (1 mol% nickel lipid). (A) Original image. (B) Deconvolved image. (C) Surface plot of intensity in deconvolved image; scale is arbitrary.

We also deconvolved images of GUVs composed of 2:2:1 DOPC:PSM:Chol with 5 mol% nickel lipid. These vesicles were subjected to the process that was described above. An example is shown in Figure S9. As reported in the main text, we found no evidence of enhanced GFP emission from the boundary, which indicates that the ehnancement seen in the 1 mol%-nickel-lipid vesicles was not a consequence of deconvolution artificacts. The lack of enhancement at this higher concentration of nickel lipid might arise from a reduced contrast between the "background" fluorescence in the L_d phase compared to the boundary.

We used artificial test images to test against deconvolution artifacts and to estimate the buildup in intensity required for detection via deconvolution. To create the test images, we first made a three-dimensional image of a one-pixel-thick vesicle with a "bite" taken out of it (*i.e.*, a circular patch was removed). This image was created in IDL (Interactive Data Language; ITT Visual Information Solutions, Boulder, CO). At the ring-shaped boundary of the "bite," the intensity was enhanced by a factor that we varied between 1 and 4.2. (An enhancement of 1 represents no enhanced fluorescence and should correspond to a control image with no accumulation of GFP at the boundary). The resultant image was convolved using an estimate of the point-spread function of our microscope. Noise was then added to

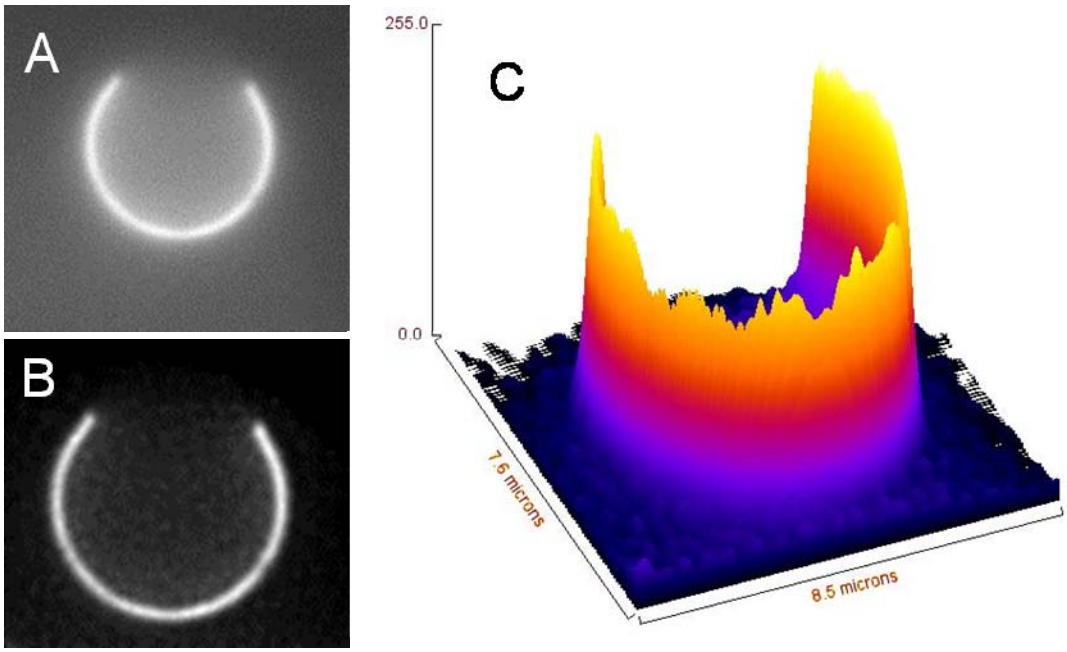

Figure S9. Deconvolution analysis of GFP fluorescence (5 mol% nickel lipid). (A) Original image. (B) Deconvolved image. (C) Surface plot of intensity in deconvolved image; scale is arbitrary.

each pixel in the amount $yI^{1/2}$ where I is the intensity of a given pixel and y is a random number drawn from a Gaussian distribution with mean of zero and a standard deviation of 1. Finally, a slice through the middle of the image was taken and deconvolved using the Huygens Essential deconvolution software. Figure S10 illustrates the deconvolution of a test image with no enhancement at the boundary. Figure S11 illustrates the deconvolution of a test image with an intensity enhancement of 4.2 at the boundary. The test images show both that the deconvolution procedure does not artificially introduce a buildup at the boundary where none exists, as evident in Figure S10, and that an enhancement of 4.2x should be detectable by our deconvolution procedure (Figure S11). Enhancements of 1.5 and 2x did not show a detectable buildup of intensity at the boundary (images not shown).

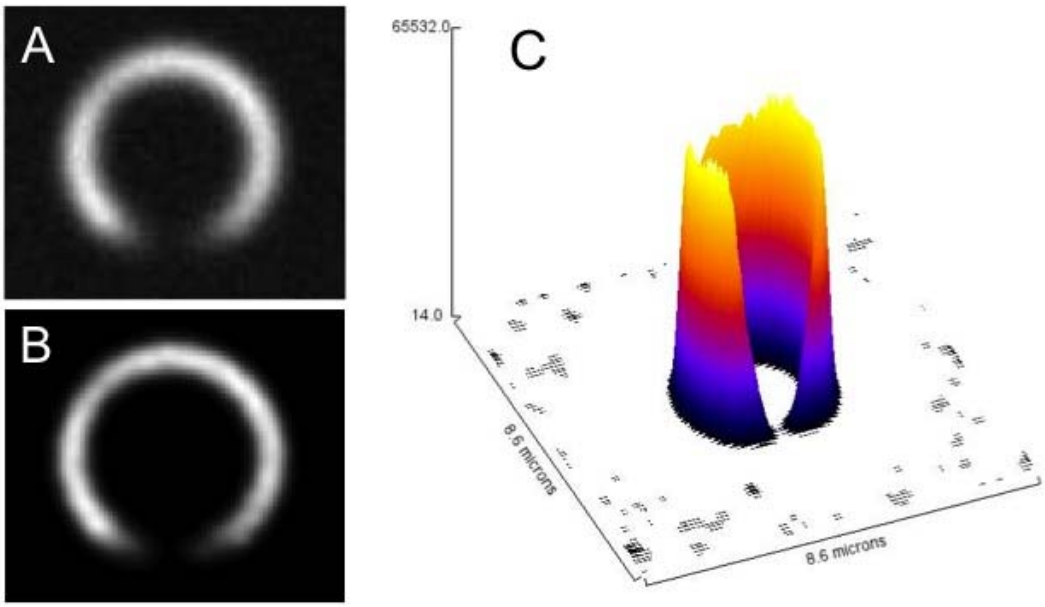

Figure S10. Deconvolution of a test image with no enhancement at the boundary. (A) Original test image. (B) Deconvolved test image. (C) Surface plot of intensity in deconvolved image; scale is arbitrary.

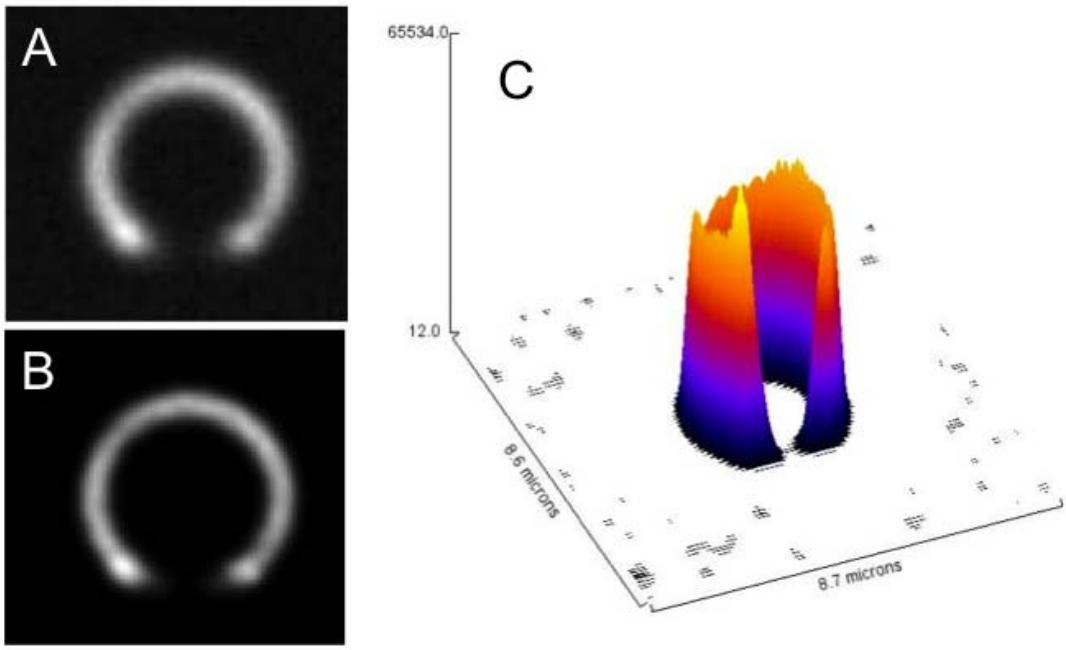

Figure S11. Deconvolution of a test image where intensity is enhanced at the boundary by a factor of 4.2. (A) Original test image. (B) Deconvolved test image. (C) Surface plot of intensity in deconvolved image; scale is arbitrary.

Supplementary Reference

(S1) Rasband, W. S.; U. S. National Institutes of Health: Bethesda, Maryland, USA, 1997-2011.